Fine-structure splittings in ^2F states of rubidium via three-step laser spectroscopy

J. R. Brandenberger, C. A. Regal,* R. O. Jung, and M. C. Yakes†
Department of Physics, Lawrence University, Appleton, Wisconsin 54912
(Received 21 August 2001; published 5 April 2002)

Three-step laser excitation is employed to measure the $^2F_{5/2}$-$^2F_{7/2}$ fine-structure splittings in seven $n\,^2F$ manifolds of Rb for $4 \leqslant n \leqslant 10$. The use of cycling transitions in the excitation process intensifies the spectra and simplifies signal detection. This sequence of seven measured splittings should serve as a useful test of fine-structure calculations in heavy alkali-metal atoms where complicated, noncentral field treatments of core polarization, configuration mixing, electron correlation, and/or relativistic effects are generally required.

DOI: 10.1103/PhysRevA.65.042510 PACS number(s): 32.10.Fn, 32.30.−r, 32.70.Jz, 39.30.+w

I. INTRODUCTION

Calculations of fine-structure splittings in alkali-metal atoms generally require treatments of core polarization, configuration mixing, electron correlation, and/or relativistic effects that go well beyond the usual central field approximations [1]. Core polarization can be viewed as a single-particle effect that arises from the exchange of the valence electron with electrons in the atomic core. The spin dependence of this interaction leads to a breaking of the spherical symmetry of the core, implying that the true stationary states for the valence electron contain substantial mixtures of the original unperturbed, single-configuration states. Electron correlation effects, which stem from the excitation of two electrons, can also be complicated and important. Relativistic corrections, especially those that pertain to the lower-lying states of heavy alkali atoms, must be included if a calculation is to be trusted up to a few percent. Taken together, these interactions can produce anomalous variations in fine-structure splittings as well as inversions in the ordering of fine-structure levels, especially in the heavier alkali-metal atoms [2–4].

Dirac's expression for the fine-structure splittings $\Delta\nu_{\mathrm{FS}}(n)$ in hydrogen can be written as $\Delta\nu_{\mathrm{FS}}(n) = \zeta(l)(1/n)^3$, where n is the principal quantum number and $\zeta(l)$ depends only upon the orbital angular momentum l. This expression reflects the effects of electron spin and relativistic dynamics, but it obviously fails to allow for electron correlation and core polarization. Since the latter effects tend to be small in lighter atoms, one might expect fine structures in the lighter alkali metals to satisfy the semiempirical generalization $\Delta\nu_{\mathrm{FS}}(n^*) = \zeta'(l)(1/n^*)^3$, where $\zeta'(l)$ is presumed to be nearly constant, $n^* \equiv n - \delta$, and δ is the quantum defect. Indeed, this expression agrees quite well with the fine-structure splittings in the ^2P, ^2D, and ^2F states of the lighter alkali metals [5]. As we show below, however, it fails to anticipate the correct sign as well as the proper trends in the magnitudes of $\Delta\nu_{\mathrm{FS}}(n)$ for the ^2F states of rubidium. These failures suggest that the inclusion of nonhydrogenic, noncentral field effects such as electron correlation and core polarization is essential to the calculation of fine-structure splittings in heavy alkali-metal atoms.

Hoping that a series of improved measurements of atomic fine structures in the alkali metals might stimulate renewed theoretical activity in this area, we have developed a three-step, laser excitation scheme that lets us measure sequences of fine-structure splittings in heavy alkali metals. This paper reports the application of this technique to measurements of the $^2F_{5/2}$-$^2F_{7/2}$ splittings in the $n\,^2F$ states of ^{85}Rb and ^{87}Rb for $4 \leqslant n \leqslant 10$. The results presented below comprise a sequence of seven fine-structure measurements, three of which are previously unmeasured, to the best of our knowledge, and four of which constitute substantially improved determinations.

II. EXPERIMENT

Seven fine-structure splittings in the $n\,^2F$ states of Rb have been measured using three-step laser excitation, the first step of which occurs on the 780.03-nm resonance line [6]. In the case of ^{87}Rb($I = \frac{3}{2}$), we excite the $5\,^2S_{1/2}(F=2)$-$5\,^2P_{3/2}(F=3)$ hyperfine transition—a strong, cycling transition that substantially populates the $5\,^2P_{3/2}$ manifold. Since the cycling nature of this transition precludes relaxation of the ^{87}Rb back into the $5\,^2S_{1/2}(F=1)$ ground state, pumping at or near the saturation intensity creates a sizable population of ^{87}Rb atoms in the $5\,^2P_{3/2}(F=3)$ state. For ^{85}Rb($I = \frac{5}{2}$), we use the $5\,^2S_{1/2}(F=3)$-$5\,^2P_{3/2}(F=4)$ transition (another cycling transition) to create a substantial $5\,^2P_{3/2}(F=4)$ population. In either case, the pumping light is provided by a 30-mW single-mode $Ga_xAl_{1-x}As$ laser diode equipped with an external cavity for tuning and line narrowing [7]. The resulting laser, which offers a spectral width of several megahertz, is locked to the desired hyperfine transition using the ditherless dichroic-atomic-vapor laser lock technique [8,9], which exploits the polarization-dependent absorption (dichroism) of a cell of Rb vapor immersed in a weak magnetic field.

The second step of excitation occurs at 1528.99 nm; it drives the $5\,^2P_{3/2}(F=3)$-$4\,^2D_{5/2}(F=4)$ transition in the case of ^{87}Rb or the $5\,^2P_{3/2}(F=4)$-$4\,^2D_{5/2}(F=5)$ transition in ^{85}Rb. These excitations represent additional cycling transitions that can pump substantial populations of Rb atoms

*Permanent address: Department of Physics, University of Colorado, Boulder, CO 80303.
†Permanent address: Department of Physics, Georgia Institute of Technology, Atlanta, GA 30332.

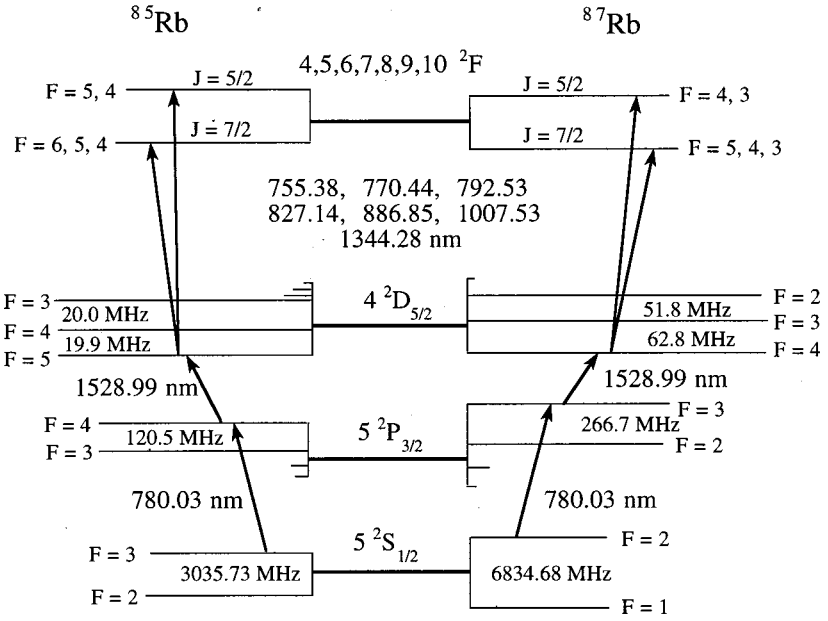

FIG. 1. Energy-level diagram showing fine and hyperfine splittings in ^{85}Rb and ^{87}Rb along with three-step excitation sequences. Note the inversion of the fine structure in the ^2F manifolds.

into the desired 4 $^2D_{5/2}$ hyperfine levels with minimal escape of atoms from the pumping cycle. Light for this second step is supplied by a commercial single-mode external-cavity diode laser [10] locked to the appropriate 1528.99-nm hyperfine transition using a small amount of dither and phase-sensitive amplification. The third wavelength in the excitation sequence is 1344.28 nm for access to the 4 ^2F state, 1007.53 nm for the 5 ^2F state, 886.85 nm for the 6 ^2F state, 827.14 nm for the 7 ^2F state, 792.53 nm for the 8 ^2F state, 770.44 nm for the 9 ^2F state, or 755.38 nm for the 10 ^2F state. To attain these wavelengths, we use seven different diodes, six of which are incorporated into external-cavity diode lasers [11]. In the case of the 10 ^2F state, we use a free-running diode laser with no cavity.

Figure 1 summarizes the pertinent energy levels and the multistep excitation scheme while Fig. 2 shows the experimental arrangement. Overlapping beams from two of the lasers copropagate while the third laser beam counterpropagates through the Rb cell, 20 cm in length. Two of the beams are horizontally polarized while the third is vertically polarized. Neutral density filters reduce the beam intensities to 100–500 μW/mm^2. The primary detector, a Si pin diode, monitors the transmission of the 780.03-nm beam passing through the cell. To facilitate locking, a Ge detector monitors the transmission of the 1528.99-nm beam. A second beam derived from the third laser drives an isolated Fabry-Perot interferometer so that interferograms and fine-structure spectra can be acquired simultaneously as the third laser scans. The lengths of the Fabry-Perot cavities, 122.26(5), 241.37(5), and 366.22(5) cm, correspond to free spectral ranges of 122.57(5), 61.47(3), and 40.92(2) MHz.

The spectral width of this three-step excitation process stems mainly from the 6 MHz natural width (full width at half maximum, FWHM) of the 780.03-nm transition and the 10–15 MHz of power broadening associated with this same transition. The second and third steps of excitation contribute less to the overall broadening because of the longer excited-state lifetimes. Dither does not broaden the excitation line-

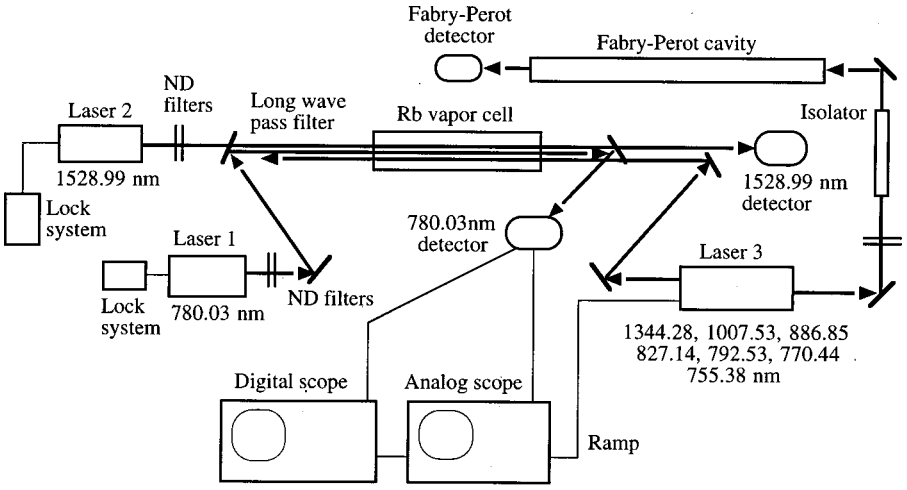

FIG. 2. Layout for three-step laser excitation spectroscopy. The ramp that sweeps laser 3 is provided by the analog scope. The digital scope records the spectra contained in the 780.03-nm beam. The symbol ND stands for neutral density filter.

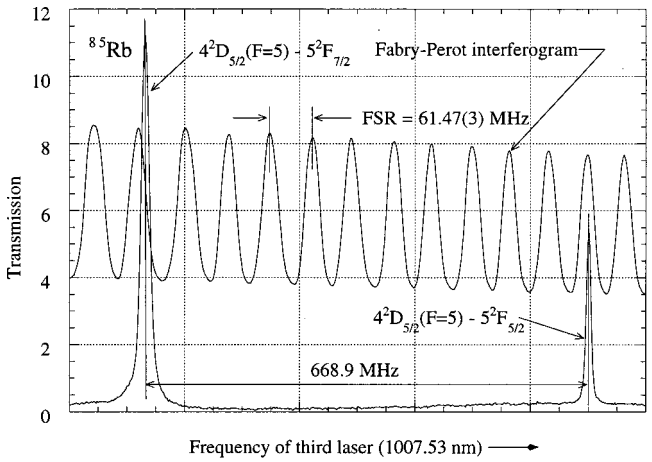

FIG. 3. Fine structure in 5 ^2F state of ^{85}Rb. Spectrum shows positive peaks in the transmission of 780.03-nm light passing through the Rb target as the 1007.53-nm beam drives the third step resonantly. Hyperfine structure cannot be resolved in this spectrum. The spectrum and Fabry-Perot interferogram are acquired simultaneously. FSR stands for free spectral range and represents the separation between adjacent interference fringes.

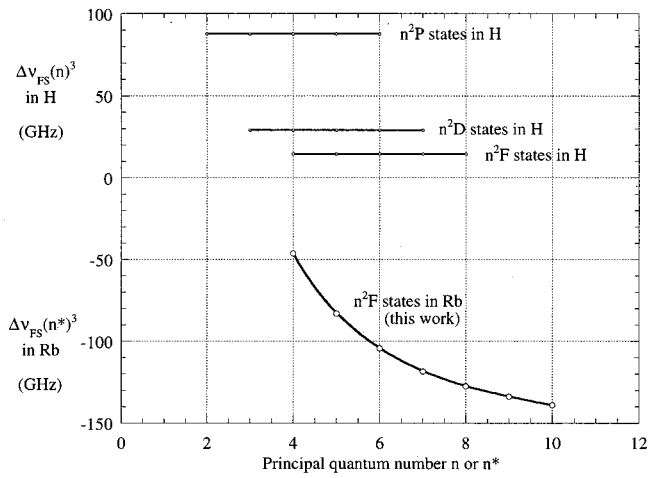

FIG. 4. Trends in the product $\Delta\upsilon_{\mathrm{FS}}(n)^3$ for various $n\ ^2P$, $n\ ^2D$, and $n\ ^2F$ states of H and the contrasting trend in $\Delta\upsilon_{\mathrm{FS}}(n^*)^3$ for ^2F states of Rb.

width since the first and third lasers require no dither and the dither of the second laser is small. It follows from these considerations that the bulk of the rubidium atoms that participate in this three-step excitation process fall in a velocity group whose members exhibit Doppler detunings of less than 20 MHz from the centers of the three resonances.

In our approach to multistep laser spectroscopy, the $n\ ^2F$ fine-structure spectra are derived from the transmission of the 780.03-nm laser beam—not from the beam of the third laser that actually sweeps through the $n\ ^2F$ fine structure. The effect of the second and third steps of excitation on the transmission of the 780.03-nm beam stems from our use of cycling transitions, which create close couplings between the populations of the involved levels. Resonances in the third step of the excitation process generate increases in the populations of the highest-lying, longest-lived levels—an effect that one observes as an increased transmission of the 780.03-nm beam due to the concomitant reduction of the $5\ ^2S_{1/2}(F=2$ or 3) population. We have observed these fine-structure resonances directly in the transmission of the third laser beam, but the signals produced in the 780.03-nm beam are larger, and they exhibit better signal-to-noise ratios.

III. RESULTS

Figure 3 shows a typical fine-structure spectrum plotted alongside its associated Fabry-Perot interferogram (the latter is used to calibrate the frequency scale of the former). Digitized versions of these signals, acquired with a dual-channel digital oscilloscope, contain 1000 samplings in the form $(y_i^{\mathrm{spectrum}}, y_i^{\mathrm{interferogram}}, t_i)$, where y_i^{spectrum} and $y_i^{\mathrm{interferogram}}$ represent signal voltages digitized simultaneously at successive instants in time t_i, and where $t_{i+1}-t_i=100\ \mu$sec. Since the frequency scan of the third laser can exhibit small nonuniformities or nonlinearities in time due to (1) competition between the resonances of the laser's internal and external cavities and (2) nonlinearity in the expansion of the piezoelectric crystal that tunes the external cavity, we calibrate each fine-structure spectrum using only that part of the associated interferogram that corresponds precisely to the separation between the spectral peaks. The use of only this part of the interferogram completely mitigates the effects of frequency nonuniformities or nonlinearities in the scanning of the laser. By processing our spectra in this manner, nonuniform laser scans produce no systematic difficulties because any scan irregularities affect both of the matched signal segments equally.

To improve our signal-to-noise-ratios, the spectra and interferograms are time averaged during each data run. Then the fine-structure splittings inferred from each of the 30 such data runs are averaged to produce a final fine-structure measurement. This method of double averaging produces fine-structure determinations reliable to about 0.1%, an uncertainty that is primarily statistical (one standard deviation of the mean). The main source of systematic uncertainty in this work stems from measuring the length of the Fabry-Perot cavity; we believe that this measurement contributes less than 0.05% uncertainty to $\Delta\nu_{\mathrm{FS}}$.

Table I contains the results of 11 determinations of fine-structure splittings between pairs of $^2F_{7/2}$ and $^2F_{5/2}$ states in ^{85}Rb and ^{87}Rb. The observed inversions in these splittings (the $^2F_{7/2}$ level always lies below the $^2F_{5/2}$ level) are indicated by the negative signs. In the four cases where we measured the splittings for both isotopes, the values are essentially indistinguishable.

Many unsuccessful attempts were made to resolve the hyperfine structure (hfs) in these spectra. We searched with special care for hyperfine splittings in the $4\ ^2F_{7/2}$ and $5\ ^2F_{7/2}$ fine-structure manifolds of ^{87}Rb, where we assumed that the hfs would be largest. These searches were hampered by the fact that the two hfs transitions that we hoped to resolve,

TABLE I. Experimental fine-structure splittings in seven $n\ ^2F$ states of Rb determined in this work and elsewhere. In those instances where measurements of $\Delta\nu_{FS}$ exist for both isotopes, we quote the average values (s_{av}) as well.

Isotope	Final state	Excitation wavelengths (nm)	Fine-structure doublet	Splitting (MHz) This work	Others
87	$4\ ^2F$	780.03			
		1528.99	$4\ ^2F_{5/2}\leftrightarrow 4\ ^2F_{7/2}$	$-728.7(5)$	$-780(300)$[a]
		1344.28			
85	$5\ ^2F$	780.03			
		1528.99	$5\ ^2F_{5/2}\leftrightarrow 5\ ^2F_{7/2}$	$-668.7(4)$	
		1007.53			
				$s_{av}=-669.1(4)$	$-570(300)$[a]
87	$5\ ^2F$	780.03			
		1528.99	$5\ ^2F_{5/2}\leftrightarrow 5\ ^2F_{7/2}$	$-669.5(4)$	
		1007.53			
87	$6\ ^2F$	780.03			
		1528.99	$6\ ^2F_{5/2}\leftrightarrow 6\ ^2F_{7/2}$	$-487.1(2)$	$-486(4)$[b]
		886.85			
85	$7\ ^2F$	780.03			
		1528.99	$7\ ^2F_{5/2}\leftrightarrow 7\ ^2F_{7/2}$	$-347.6(4)$	
		827.14			
				$s_{av}=-347.3(2)$	$-347.6(10)$[b]
87	$7\ ^2F$	780.03			
		1528.99	$7\ ^2F_{5/2}\leftrightarrow 7\ ^2F_{7/2}$	$-347.1(2)$	
		827.14			
85	$8\ ^2F$	780.03			
		1528.99	$8\ ^2F_{5/2}\leftrightarrow 8\ ^2F_{7/2}$	$-250.7(4)$	
		792.53			
				$s_{av}=-250.5(2)$	$-150(300)$[a]
87	$8\ ^2F$	780.03			
		1528.99	$8\ ^2F_{5/2}\leftrightarrow 8\ ^2F_{7/2}$	$-250.3(2)$	
		792.53			
85	$9\ ^2F$	780.03			
		1528.99	$9\ ^2F_{5/2}\leftrightarrow 9\ ^2F_{7/2}$	$-184.6(3)$	
		770.44			
				$s_{av}=-184.5(2)$	
87	$9\ ^2F$	780.03			
		1528.99	$9\ ^2F_{5/2}\leftrightarrow 9\ ^2F_{7/2}$	$-184.5(2)$	
		770.44			
87	$10\ ^2F$	780.03			
		1528.99	$10\ ^2F_{5/2}\leftrightarrow 10\ ^2F_{7/2}$	$-139.9(15)$	
		755.38			

[a]Reference [12].
[b]Reference [5].

namely, the $4\ ^2D_{5/2}(F=4)$-$n\ ^2F_{7/2}(F=4,5)$ transitions, differ considerably in line strength [13]. This consideration, when combined with the observed 20–25 MHz widths (FWHM) of our fine-structure features and the high degree of symmetry in our experimental line shapes, suggests that the unresolved hfs in the 4, $5\ ^2F$ manifolds must be less than 10 MHz. We continue to search for methods that will permit resolution of these hyperfine splittings.

IV. DISCUSSION

Table I also compares the 11 fine-structure splittings determined in this work to previous measurements. With one exception, our measurements are one or two orders of magnitude more precise than those of previous investigators. Our multistep technique, which differs from one ^2F manifold to another only by the wavelength of the third laser, offers the prospect of good internal consistency from one fine-structure

measurement to the next. In the case of previous determinations, three were performed by conventional optical spectroscopy [12]; the quoted overall uncertainties in these particular determinations were about 50%. The other two determinations, completed by Farley and Gupta [5], employed radio-frequency spectroscopy. Their quoted uncertainties are 1% and 0.3%.

As mentioned in Sec. I, hydrogenic fine-structure splittings satisfy the expression $\Delta\nu_{\mathrm{FS}}(n)n^3=\zeta(l)$, where $\zeta(l)$ is constant for a given value of l. Figure 4 compares the products $\Delta\nu_{\mathrm{FS}}(n)n^3$ for three hydrogenic cases [14] to the corresponding product $\Delta\nu_{\mathrm{FS}}(n^*)(n^*)^3$ applicable to the $n\ ^2F$ splittings measured in this work. The comparison is quite revealing: (1) the product $\Delta\nu_{\mathrm{FS}}(n^*)(n^*)^3$ for Rb fails to exhibit a constant or near-constant value for $\zeta'(l)$, in sharp contrast to the hydrogenic cases; (2) the signs of $\Delta\nu_{\mathrm{FS}}$ for Rb are uniformly negative, in agreement with the well-known fact that the $n\ ^2F$ fine structures in Rb are inverted; (3) there is no indication that the negative values of these $\Delta\nu_{\mathrm{FS}}$ for Rb are likely to change sign at some larger value of n; and (4) the absolute magnitudes of the products $\Delta\upsilon_{\mathrm{FS}}(n^*)(n^*)^3$ in the $n\ ^2F$ states of Rb are substantially larger than their $n\ ^2F$ hydrogenic counterparts.

Various authors [1–4] have invoked core polarization, correlation effects, and/or relativistic treatments to calculate fine-structure splittings in both light and heavy alkali atoms. Some of these attempts have accounted successfully for the inversion of the fine structures in certain states, but to date no one has attempted detailed calculations of the fine structures of the $n\ ^2F$ states of rubidium. Further investigation of this situation in Rb must await new efforts to calculate these fine-structure splittings.

ACKNOWLEDGMENTS

This work was supported by the Research Corporation and Lawrence University. We are pleased to acknowledge the original suggestions and timely contributions of Stephen R. Lundeen at numerous stages of this work.

[1] I. Lindgren and Ann-Marie Mårtensson, Phys. Rev. A **26**, 3249 (1982).
[2] E. Luc-Koenig, Phys. Rev. A **13**, 2114 (1976); J. Phys. (Paris) **41**, 1273 (1980).
[3] T. Lee, J. E. Rodgers, T. P. Das, and R. M. Sternheimer, Phys. Rev. A **14**, 51 (1976); R. M. Sternheimer, J. E. Rodgers, T. Lee, and T. P. Das, *ibid.* **14**, 1595 (1976).
[4] N. C. Pyper and P. Marketos, J. Phys. B **14**, 4469 (1981).
[5] J. W. Farley and R. Gupta, Phys. Rev. A **15**, 1952 (1977).
[6] All wavelengths quoted in this paper are measured in air.
[7] This external-cavity laser represents our own design. It is tunable over ±5 nm and employs a Sharp LT024MD0 laser diode selected to lase within 3 nm of 780 nm. Such diodes are available from Thorlabs, Inc.
[8] V. V. Yashchuk, D. Budker, and J. R. Davis, Rev. Sci. Instrum. **71**, 341 (2000).
[9] K. L. Corwin *et al.*, Appl. Opt. **37**, 3295 (1998).
[10] This diode-based laser is a 10-mW Vortex model manufactured by New Focus, Inc.
[11] The diodes employed in these external-cavity lasers provide free-running output powers of 20–50 mW. All diodes are index-guided, single transverse-mode devices supplied by distributors such as Toptica GmbH, Polytec PI, Dora Texas Corp., Frankfurt Laser, Optima Precision, Roithner Lasertechnique, and Thorlabs, Inc. In some instances, the manufacturers of these devices have recognizable names such as Sharp, Hitachi, Sanyo, Mitsubishi, etc., but in other instances the distributors do not reveal the names of the manufacturers.
[12] I. Johansson, Ark. Fys. **20**, 135 (1961).
[13] The predicted relative strengths of these lines arse 8.8 and 100.0 according to tabulated calculations that initially appeared in H. E. White and A. Y. Eliason, Phys. Rev. **44**, 753 (1933).
[14] The hydrogenic values of $\zeta(l)$ shown in Fig. 4 are calculated using Dirac's expression.